PHYSICAL REVIEW A **75**, 030701(R) (2007)

Angular-momentum-dependent Fano profiles in excited zinc atoms

L. Pravica,[1,2,*] D. Cvejanović,[1,2] J. F. Williams,[1,2] and S. A. Napier[1]
[1]*Centre for Atomic Molecular and Surface Physics, Physics Department, University of Western Australia, Perth 6009, Australia*
[2]*ARC Centre for Antimatter-Matter Studies, Physics Department, University of Western Australia, Perth 6009, Australia*
(Received 22 August 2006; published 8 March 2007)

The Fano-equivalent profiles of two negative-ion resonant states have been observed in the integrated Stokes parameters of 636.2 nm photons emitted from the $3d^{10}4s4d\ ^1D_2$ state of zinc. These profiles reflect the effects of electron exchange and the spin-orbit interaction via the angular-momentum-dependent properties of the alignment and orientation Stokes parameters. The resonant states have energies of 10.98 ± 0.02 eV and 11.33 ± 0.02 eV and widths of 0.25 ± 0.03 eV and 0.33 ± 0.05 eV, respectively, and are bound to an excited atomic state with a $3d^9$ core hole. The lower-energy resonance shows a strong spin-orbit interaction whereas the higher-energy resonance shows negligible spin-orbit interaction.

DOI: 10.1103/PhysRevA.75.030701 PACS number(s): 34.80.Dp

Interference is a universal phenomenon in physics, be it classically between two waves or quantum mechanically, for example, between a bound and a continuum state of an atom. The interchannel interference observed here is a many-body effect produced by a coupling of direct and continuum electronic configurations excited by electron impact, which gives rise to a characteristic Fano profile [1]. The profile is seen in many diverse areas of atomic, nuclear, and condensed matter physics and recently in cold-atom Efimov states [2]. Its value lies in the insight it gives into the physical interaction mechanisms [3], spectroscopy [4], and reaction dynamics [5] of the interacting systems. Other examples occur in the time domain by evolution of attosecond electronic wave packets [6] and in electron transport through a quantum dot molecule, where coherence is preserved [7] and the conductance spectrum between bonding and antibonding states shows a Fano resonance whose width indicates the lifetime of the molecule [8]. The present study explores angular momentum effects in atomic physics, particularly in the region of resonances and using incident spin-polarized electrons which under certain conditions enables electron exchange and spin-orbit interaction effects to be separated by observation of the Stokes parameters [9,10].

Most studies of Fano profiles have led to the identification and characterization of spectral series. For example, the classic Fano profile occurs for photoabsorption in helium from about 19 to 21 nm as a result of interference between direct photoionization and double-excitation processes. The analysis of the line shape and energy characterized the angular momenta of states with mixed electronic configurations of the type $2snp\ ^1P_1 \pm 2pns\ ^1P_1$. However, details of the spin and orbital angular momentum effects have been identified infrequently in Fano profiles. Perhaps the most explicit and informative characterization has emerged from the total photon absorption cross section by Glass-Maujean and Siebbeles [11]. For linearly polarized photons exciting randomly oriented molecules, they showed that along an asymmetric Fano profile the continuum, resonance, and interference terms have different angular asymmetry β parameters and that those parameters depend on the electron couplings and correlations as well as phase differences between excitation amplitudes. Similar variations of β and electron spin polarization were observed in the photoionization of zinc [12]. Those experimental observations were limited by dipole synchrotron radiation. For electron impact, with increased degrees of freedom over photon impact, Defrance [13] has shown in helium how a Fano profile, or the frequently applied representations of Fano and Cooper [14], in the polarization of cascade atomic radiation characterizes autoionizing states of excited negative ions. The characterization of the states near 58 eV was in agreement with that obtained by Fano and Cooper [15] combining elements of spectroscopy and scattering theory. However, unresolved questions remained concerning how electron coupling schemes, correlations, and configuration interactions, and the spin and orbital angular momenta in the autoionizing states, affected the Fano profiles.

The spin-orbit and electron exchange effects can be identified via the measured Stokes parameters, not only in the excited state but also in the resonance state [10]. In this Rapid Communication we apply this technique and investigate the spin-dependent effects in two negative-ion resonance states overlapping the ionization continuum in zinc which are advantageously observed in 636.2 nm decay radiation from the $4d\ ^1D_2$ state of zinc after their autoionization. The resonances were clearly distinguishable in the measured polarizations but not in the individual intensities of the 636.2 nm radiation. The profiles were fitted with a Fano-equivalent Shore parametrization [16] which allowed classification of the resonances in terms of energy and width. Analysis of the Stokes parameters then yielded characteristics of the resonances such as configuration, coupling scheme, the effects of electron exchange and spin-orbit interaction, and angular momentum transfer mechanisms.

The scattering process investigated is described by the following representation:

$$\begin{aligned} \mathrm{Zn}(3d^{10}4s^2\ ^1S_0) + e(\uparrow\downarrow) &\rightarrow \mathrm{Zn}^{*-}(3d^9 4s^2 4p^2) \\ &\rightarrow \mathrm{Zn}(3d^{10}4s4d\ ^1D_2) + e \\ &\rightarrow \mathrm{Zn}(3d^{10}4s4p\ ^1P_1) + h\nu + e. \end{aligned}$$

*Electronic address: luka@physics.uwa.edu.au

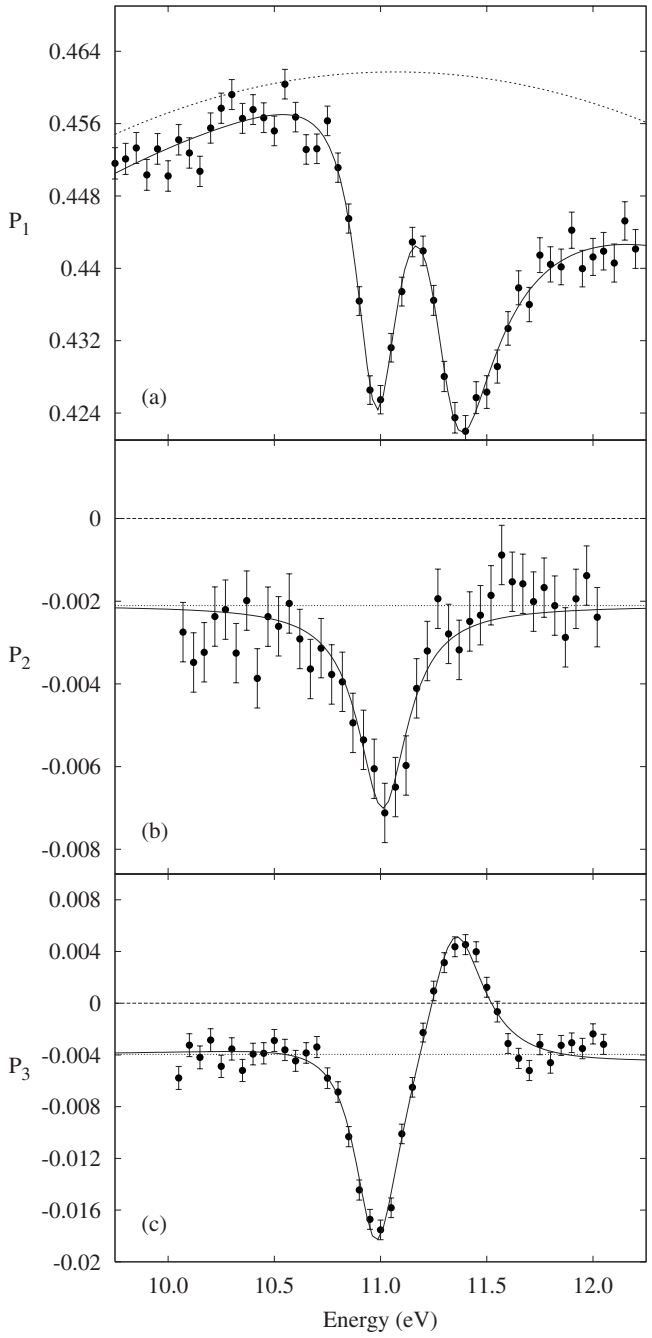

FIG. 1. Stokes parameters P_1, P_2, and P_3. Solid line: fit to the Fano profile. Dotted line: fit to the polarization background.

An electron temporarily is bound to an excited atomic state with a vacancy in the $3d$ subshell which adds a new avenue for studying configuration interactions and which is expected to enhance the spin-dependent effects.

The appropriate experimental symmetries for excitation and observation use the geometry shown in Fig. 1 of [17]. The linear momentum vector and the spin vector of the transversely polarized incident electrons define the z and y axes, respectively, of a right-handed rectilinear coordinate system. The scattered and ejected electrons are not detected, and the integrated Stokes parameters are defined in terms of the photon intensities observed along the y axis such that

TABLE I. Energy E and width Γ for the two observed resonances as obtained from fitting the resonance profiles to the Stokes parameters P_1, P_2, and P_3 of Fig. 1. An additional uncertainty from the energy calibration of ±50 meV applies to the resonance energies.

Stokes parameter	Lower-energy resonance		Higher-energy resonance	
	E_1 (eV)	Γ_1 (eV)	E_2 (eV)	Γ_2 (eV)
P_1	10.97±0.02	0.25±0.03	11.31±0.02	0.33±0.05
P_2	11.01±0.02	0.28±0.05		
P_3	10.97±0.02	0.26±0.03	11.35±0.03	0.34±0.06

$P_1=\frac{I(0°)-I(90°)}{I(0°)+I(90°)}$, $P_2=\frac{I(45°)-I(135°)}{I(45°)+I(135°)}$, and $P_3=\frac{I(\sigma^-)-I(\sigma^+)}{I(\sigma^-)+I(\sigma^+)}$ where $I(\theta)$ is the intensity of photons with a polarization angle θ with respect to the z axis and $I(\sigma^+)$ and $I(\sigma^-)$ are, respectively, the intensities of photons with positive and negative helicity.

For the incident spin-polarized electrons, the incident electron spin angular momentum and linear momentum vectors define a planar scattering symmetry and the three Stokes parameters P_1, P_2, and P_3 describe the asymmetries of the polarization pattern of the emitted radiation. Then P_2 can be related to the spin-orbit interaction and P_3 to the spin-orbit interaction and the electron exchange [10]. The remaining parameter P_1 does not depend on the spin of incident electrons because of cylindrical symmetry. The validity of this approach and these "integrated" Stokes parameters measurements have been confirmed by Wolcke *et al.* [18] and in our laboratory for inner-shell excitation in zinc [19] and in neon [20].

Our crossed electron-atom beam apparatus is an improved version of that described earlier [17]. The energy spread and electron polarization were about 180 meV and 30% for the measurement of P_1 and 250 meV and 66% for the P_2 and P_3 measurements. The energy scale was calibrated to within 50 meV by fitting the sharp photon excitation function at threshold to the theoretical integral cross section [21] convoluted with a Gaussian apparatus function.

The measured Stokes parameters (normalized to the incident electron polarization) of the 636.2 nm photons from the $4s4d\ ^1D_2$ state are shown in Fig. 1. P_3 and P_1 clearly show two features superimposed on a polarization background caused by direct excitation while P_2 is affected only by the

TABLE II. Fano q parameters for the two observed resonances with $^2D_{5/2}$ and $^2D_{3/2}$ ion cores as obtained from the fitting of intensities for different light polarizations. I_1 corresponds to light intensities at 0°, 45°, and σ^+ and I_2 corresponds to light intensities at 90°, 135°, and σ^- for P_1, P_2, and P_3, respectively.

Stokes parameter	Lower-energy resonance		Higher-energy resonance	
	I_1	I_2	I_1	I_2
P_1	10.0	12.0	−1.6	−7.1
P_2	4.5	4.4	−2.1	−2.1
P_3	4.5	3.9	−1.8	−2.8

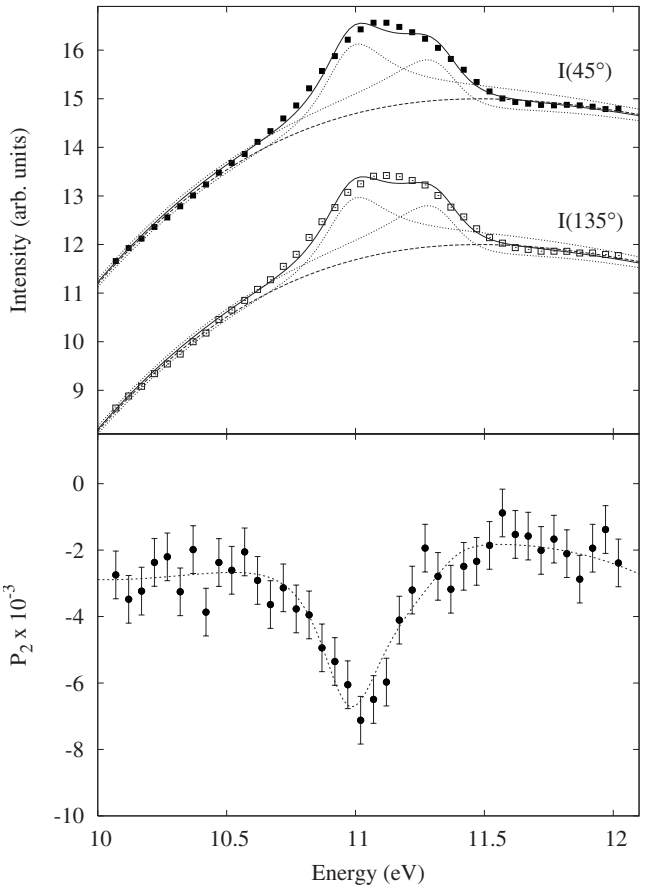

FIG. 2. Top: measured photon intensities $I(45°)$ (■) and $I(135°)$ (□); dashed line, the contribution of direct scattering (DS); dotted lines, fitted individual resonances + DS; solid line, sum of resonance fits and DS. $I(135°)$ was offset relative to $I(45°)$ for clarity reasons. Bottom: Stokes parameter P_2; the dashed line is calculated from the fitted intensities.

lower-energy resonance. Each of the resonance structures was fitted using the Shore parametrization $\frac{a\epsilon+b}{1+\epsilon^2}$, where a and b are the Shore parameters [16] which characterize the shape of the resonance and ϵ is defined as $\epsilon=2(E-E_r)/\Gamma$, where E is the incident electron energy, E_r is the resonance energy, and Γ is the resonance width. The Fano q parameters can be calculated using $q=\frac{b\pm\sqrt{a^2+b^2}}{a}$, where $\mathrm{sgn}(q)\equiv\mathrm{sgn}(a)$.

As the resonances were not resolved in the photon intensities, their energies and widths were determined from the fits of the Fano profiles to the polarizations. The resulting E and Γ are shown in Table I. The fitting of Fano profiles to the polarization is justified only when the Fano q parameters of a resonance observed in two different polarized photon intensities, e.g., $I(45°)$ and $I(135°)$ for P_2, have the same order of magnitude [13]. This is the case here, as shown below.

Next, the energies and the widths from the fits to polarizations were used to fit each of the six intensity curves to obtain Fano q parameters for each resonance. This is shown in Table II. The fits to the intensities were then used to calculate the Stokes parameters. Although the individual intensities show unresolved contributions by both resonances, a remarkable agreement was obtained even for P_2, shown in Fig. 2, the most complex and least statistically accurate measurement. The calculated P_2 values reproduce the single lower-energy resonance with a shape and energy in excellent agreement with the measured P_2 shown in Fig. 1(b). The same level of agreement and accuracy is obtained by applying the procedure to the polarization parameters P_1 and P_3. We assume that there is no interference between the two resonances which we term as the lower (10.98±0.02 eV) and higher (11.33±0.02 eV) energy resonances.

Further analysis of the resonances requires a discussion of likely configurations and coupling schemes and of the effects of electron exchange and the spin-orbit interaction as well as the angular momentum transfer mechanisms. An electronic configuration can be derived from the assumption that the additional electron is bound in the field of a known excited state with a negative electron affinity of up to approximately 0.5 eV. The energy levels in the autoionizing region of relevance here [22] are shown in Fig. 3. Similar to the approach used for heavy noble gases [23] and some other atoms [24], the resonance energies are compared with the calculated center-of-gravity energies (CGEs) of states from the nearby $3d^{10}4p^2$ (CGE=10.301 eV) and $3d^9 4s^2 4p$ (CGE =11.459 eV) configurations, as shown in Fig. 3. This approach indicates that $3d^9 4s^2 4p$ is the most probable configuration for the observed resonances as the majority of the doubly excited $3d^{10}4p^2$ configuration states are too low in energy. We propose an assignment for the lower- and higher-energy resonances in which the negative ion consists of two outermost $4p$ electrons bound to $3d^9 4s^2$ $J=5/2$ and $J=3/2$ ion cores, respectively. Spin-orbit splitting in this ion core is 0.337 eV [25] in accordance with the energy difference of 0.36±0.02 eV between the two observed resonance structures. Without further experiments and theoretical calculations the assignment of angular momentum can only be speculated because of the large number of possible states arising from this configuration.

The resonance structures in P_2 and P_3 provide information on momentum couplings and the role of spin-dependent interactions (spin-orbit and electron exchange) [10] in these

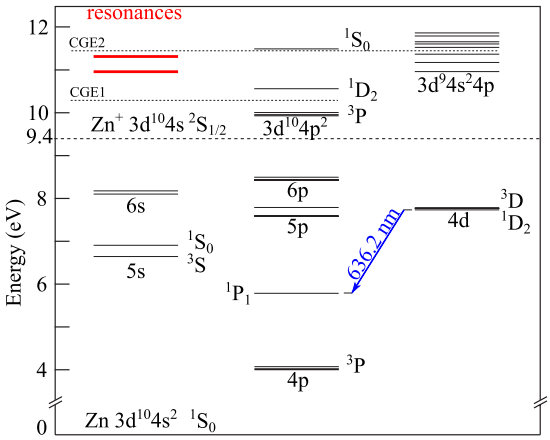

FIG. 3. (Color online) Energy-level diagram of zinc showing the observed 636.2 nm transition, the observed resonance energies above ionization threshold, and two doubly excited neutral series. CGE1 and CGE2 are the center-of-gravity energies for the $3d^{10}4s^2$ and $3d^9 4s^2 4p$ multiplets, respectively.

highly correlated temporary complexes. While the spin-orbit interaction with the continuum electron is negligible for zinc atoms, this may not be true for the target electron and it can lead to the breakdown of the *LS*-coupling scheme. This distinction is important in negative ions as the continuum electron becomes a bound "atomic" electron for the lifetime of the negative ion [26]. The nonzero values of P_2 in the region of the lower-energy ($J=5/2$ core) resonance are an indication of the existence of a weak, but measurable, spin-orbit interaction within the negative ion and the breakdown of *LS*-coupling. The zero values of P_2 for the higher-energy ($J=3/2$ core) resonance indicate negligible spin-orbit interaction and the validity of *LS*-coupling.

Nonzero values of P_3 can be caused by the spin-orbit and exchange interactions [10]. The opposite signs of the resonances in P_3 are explained as follows. If exchange is the dominant spin-dependent interaction, then the electron spin-polarization vector $\vec{P}$ and P_3 will have the same sign for the studied transition. A change in sign can be caused only by spin-orbit interaction in the collision. The fact that the lower-energy resonance has P_3 with an opposite (negative) sign from the spin-polarization vector is an indication that the spin-orbit interaction is dominant over exchange. Therefore, both spin-dependent parameters P_2 and P_3 reveal in a consistent way the lower-energy resonant state to be dominated by a spin-orbit interaction (negative P_3 and a resonance in P_2) and the higher-energy resonance to be dominated by exchange (positive P_3 and no resonance in P_2).

In conclusion, we have observed the Fano profiles caused by two temporary negative-ion states of zinc via measurements of the Stokes polarization parameters from the decay of the $4s4d\ ^1D_2$ neutral state. The Stokes parameters revealed significantly more details than the emission cross sections and allowed the two resonances to be resolved. They also identified the dominant roles of electron exchange and the spin-orbit interaction and have shown how the spin-orbit interaction is related to the total angular momentum of the ion core of the resonance state. With prophetic insight Fano [27] long ago described the spin-orbit interaction as a "weak force with conspicuous effects." The use of spin-polarized incident electrons enabled the integral polarization technique to be used to explore measurable effects of these weak magnetic interactions. Future work will concern the observation of these resonance structures in different exit channels and in angular differential modes to obtain information on phase shifts and a theoretical description of the structure and dynamical behavior.

This work was supported by the University of Western Australia. S.N. is supported by APA.

[1] U. Fano, Phys. Rev. **124**, 1866 (1961).
[2] I. Mazumdar, A. R. P. Rau, and V. S. Bhasin, Phys. Rev. Lett. **97**, 062503 (2006).
[3] P. Courteille, R. S. Freeland, D. J. Heinzen, F. A. van Abeelen, and B. J. Verhaar, Phys. Rev. Lett. **81**, 69 (1998).
[4] C. A. Regal, M. Greiner, and D. S. Jin, Phys. Rev. Lett. **92**, 040403 (2004).
[5] R. Bruhn, E. Schmidt, H. Schroder, and B. Sonntag, J. Phys. B **15**, 2807 (1982).
[6] M. Wickenhauser, J. Burgdorfer, F. Krausz, and M. Drescher, Phys. Rev. Lett. **94**, 023002 (2005).
[7] A. A. Clerk, X. Waintal, and P. W. Brouwer, Phys. Rev. Lett. **86**, 4636 (2001).
[8] M. L. LadrondeGuevara, F. Claro, and P. A. Orellana, Phys. Rev. B **67**, 195335 (2003).
[9] K. Bartschat, K. Blum, G. F. Hanne, and J. Kessler, J. Phys. B **14**, 3761 (1981).
[10] K. Bartschat and K. Blum, Z. Phys. A **304**, 85 (1982).
[11] M. Glass-Maujean and L. D. A. Siebbeles, Phys. Rev. A **44**, 1577 (1991).
[12] R. Kuntze, N. Böwering, M. Salzmann, U. Heinzmann, and N. L. S. Martin, J. Phys. B **29**, 1025 (1996).
[13] A. Defrance, J. Phys. B **13**, 1229 (1980).
[14] U. Fano and J. W. Cooper, Phys. Rev. **137**, A1364 (1965).
[15] U. Fano and J. W. Cooper, Phys. Rev. **138**, A400 (1965).
[16] B. W. Shore, J. Opt. Soc. Am. **57**, 881 (1967).
[17] P. A. Hayes, D. H. Yu, J. Furst, M. Donath, and J. F. Williams, J. Phys. B **29**, 3989 (1996).
[18] A. Wolcke, K. Bartschat, K. Blum, H. Borgmann, G. F. Hanne, and J. Kessler, J. Phys. B **16**, 639 (1983).
[19] D. H. Yu, L. Pravica, J. F. Williams, N. Warrington, and P. A. Hayes, J. Phys. B **34**, 3899 (2001).
[20] D. H. Yu, P. A. Hayes, and J. F. Williams, J. Phys. B **30**, L487 (1997).
[21] O. Zatsarinny and K. Bartschat, Phys. Rev. A **71**, 022716 (2005).
[22] M. W. D. Mansfield, J. Phys. B **14**, 2781 (1981).
[23] F. H. Read, J. N. H. Brunt, and G. C. King, J. Phys. B **9**, 2209 (1976).
[24] S. J. Buckman and C. W. Clark, Rev. Mod. Phys. **66**, 539 (1994).
[25] NIST Atmoic Spectra Database 2006 Web site, URL {http://physics.nist.gov/PhysRefData/ASD}.
[26] G. F. Hanne, Phys. Rep. **95**, 95 (1983).
[27] U. Fano, Comments At. Mol. Phys. **2**, 30 (1970).